Chapter 7

Characterization of Carbon Nanotubes

Rolant Eba Medjo

Additional information is available at the end of the chapter

http://dx.doi.org/10.5772/51540

1. Introduction

Carbon is one of the most abundant and most fascinating elements on earth. It appears in several different forms or allotropes with widely different properties. Among these allotropes are diamond, graphite and amorphous carbon. It forms also a great variety of novel structures that are being discovered day after day these last years. The discovery of novel carbon allotropes or *carbon nanostructures* (CNSs) has attracted intensive attention due to their fundamental and technological interests [1, 2]. They exhibit unique structural and physical properties. Carbon nanostructures are promising to revolutionize several fields of fundamental science and contribute as major component of nanotechnology. Previous studies have shown that these nanostructures can be used in composite materials or in individual functional elements of nanodevices such as: hydrogen storage, nanomanipulation, medical usages and nonporous membranes [3]. Such devices imply precise demands as high aspect ratio, vertical alignment on flat plan and electronic conductivity among the properties of CNSs. Special attention is now devoted to electrons or field emission. But there still remains a wide range of unexplored potential applications in various nanotechnological areas such as aerospace, energy, automobile, medicine, or chemical industry, in which CNSs can be used as gas adsorbents, templates, actuators, composite reinforcements, catalyst supports, probes, sensors, nanopipes and nanoreactors. Besides the attractive aspects of carbon nanostructures, their synthesis is complex compared to other materials used in different domains of technology and different existing methods of synthesizing. These methods lead to CNSs with sometimes an important quantity of impurities incorporated, encapsulated or adsorbed, whose amount and types depend on techniques and parameters of synthesis.

Among carbon nanostructures, CNTs are the most important because they possess the most determinant properties for revolutionary applications. Proprieties exhibited by CNTs are in

general given qualitatively by electron microscopies. However, SEM examination provides an overview of nanostructures, and a more accurate examination by TEM generally reveals many defects [4]. All these microscopies very often, mask some observations of CNTs arrangements. The controlling or characterization is also done qualitatively by very few other techniques, often used to more deeply investigate the morphology and the structure, such grazing-incidence small-angle X-ray scattering (GISAXS) [5]. This technique is semi-quantitative. It is part of those which allow an in situ and real time study of islands growing on a substrate and give access to their third dimension. This aspect is the most important when the use of imagery techniques becomes difficult and impossible. It gives structural and morphological information and correlations on CNTs and their mutual orientation. The obtained results are in agreement with the qualitative ones from SEM and TEM. GISAXS is an extension of the well knows SAXS (Small Angle X-ray Scattering). XANES spectroscopy has been a powerful tool that not only provides information on the local environment around carbon, such as diamond, carbon nitride and graphitic carbon [6-8], but also investigates the absorption and adsorption of hydrocarbon molecules [9], radicals and atoms with specific selectivity for the orientation of these compounds. This property of XANES spectroscopy is due to the angular dependence of the absorption transition [6]. XANES is a local probe, sensitive to chemical impurities, defects, chemical adsorption and curvature induced orbital rehybridization.

In this chapter are presented characterization techniques of carbon nanotubes notably electron microscopies and XANES spectroscopy. Later, electron microscopy images analysis is done. XANES spectra are quantitatively analyzed. It ends with a conclusion.

2. Characterization Techniques

Electron microscopy is an imaging technique that uses an electron beam in order to probe a material. Since the wavelength of an electron is much smaller than the wavelength of visible light, diffraction effects occur at much smaller physical dimensions. The microscope was the first tool by means of which a real study could be made of objects too small to be seen with the naked eye. From its crude beginning some 300 years ago, it has been developed into an instrument that is a credit to the inventive skill and analytical ability of those that have worked on it. The modern microscope is an instrument that approaches the "theoretical limit" of its performance, the information that can be extracted from High Resolution Transmission Electron Microscopy (HRTEM) is not straight-forward since the preparation of TEM samples may mask some observation of CNTs arrangements. A great variety of experiments has been carefully done to give the properties of the atoms, molecules, electrons, protons... regarded as the constituents of matter. The limitation on the performance of a microscope is set by its resolving power. Further characterization tools are desirable especially those which are not destructive for the samples to complete electron microscopy studies. Among these tools are cited:

- the scanning tunnelling microscopy (STM),
- the atomic force microscopy (AFM),
- the X-ray photoemission spectroscopy (XPS),
- the grazing incidence small angles X-ray scattering
- the X-ray absorption near-edge structure spectroscopy.
- the Raman spectroscopy.

It has been shown that nuclear magnetic resonance (NMR) and XANES have proved to be the most powerful ones in detecting and resolving the various bonding environments. The main drawback of NMR is that it requires detaching and powderizing the coating until reaching a relatively large amount of sample. XANES, instead, can be performed on a single coating without any sample preparation.

2.1. Electron Microscopy

Electron microscopy is an essential tool for characterizing any nanomaterial because it allows direct observation of size, shape, structure. The local structure of the CNSs can be investigated at the nanometer and subnanometer level by TEM, SEM, AFM and STM. TEM and SEM are useful tools to check the exfoliation of bundles and the purity of the material. However TEM and SEM produce damages on the sample due to the use of the electron beam.

Electron Microscopy was developed due to the limitations of Light Microscopy which is limited by the physics of light to 500 or 1,000 times magnification and a resolution of 0.2 micrometer. In the early of the 1930 decade, this theoretical limit had been reached and there was a scientific desire to see the fine details of the interior structures of organic cells. Electron Microscopy is a scientific technique used to examine objects on a very fine scale. This thin specimen is irradiated with an electron beam of uniform current density.

This required 10,000 times magnification which was not possible to be obtained using Light Microscopes.

Electron Microscopes operate exactly as their optical counterpart except that they use a focused beam of electrons instead of light to "image" the specimen and gain information about its structure and composition.

There are two types of electron microscopy, namely the transmission electron microscopy and the scanning electron microscopy.

The information that TEM or SEM examination can yield are the following:

- The topographical information: the surface features of an object or "how it looks", its texture.
- The morphological information: the shape and size of the particles making up the object.
- The composition information: the elements and compounds that the object is composed of and the relative amounts of them

The relationship is direct between these information and the material properties.

The crystallographic information itemizes how the atoms are arranged in the object and provides direct relation between these arrangements and materials properties is given only by TEM.

There are two main constrains for the sample observation in Electron Microscopy. The first is that the sample should be stable in the vacuum. The second, the sample must be under the electron beam. Other specific limitations have to be fulfilled in each Electron Microscopy.

The critical point of the study of CNSs is their direct observation limitation by the use of HRTEM. The information that can be extracted is not straight-forward since preparation of TEM specimens may mask the observation nanostructure arrangements. For example, during ion beam milling for cross-section imaging preparation, high ion bombardment may destroy the structure due to surface amorphization. These drawbacks may be overcome by the reduction of the ion bombardment in the final steps of the thinning process or by studying plan-view specimens when deposition on soluble substrates is possible.

Another problem in HRTEM analysis comes from projection of artefacts, which may preclude the resolution of structural features. This can be partially solved by considering selective area electron diffraction (SAED), since any overlapping does not affect the characteristic lattice spacing in the diffraction pattern and information on the degree of ordering can be derived from the brightness and width of the diffraction pattern.

Finally, an additional drawback of TEM measurements for studying films is the destructive character entailed. Further identification of CNTs with additional characterization tools is required, especially if they are not destructive for the sample. In the next section, we present XANES spectroscopy.

2.2. X-ray absorption near edge structure spectroscopy

X-ray absorption near-edge structure also called NEXAFS (near-edge X-ray absorption fine structure) exists in the energy level of 50 eV above the absorption edge. It includes the unoccupied part of band structure just above the Fermi level. Thus, certain aspects of electronic structure of detected element can be revealed.

X-ray absorption spectroscopy in general, has gained much of its reputation of being a powerful analytical and research tool, mostly due to the use of synchrotron radiation sources. In this kind of spectroscopy, interactions between photons and matter are studied by measuring the photoabsorption cross-section. The absorption of X-ray creates the photon-induced excitations of an electron from a core state to an empty state above the Fermi level. This absorption is measured as a function of photon energy, close to a core level binding energy. The intensity of X-ray beam passing through a sample (Figure 1b) of thickness d is given by the Beer Lambert law:

$$I = I_0 e^{-\mu(E)d} \tag{1}$$

where is the beam intensity hitting the sample and I the intensity transmitted through the material.

XAS provides valuable information about the electronic structure by probing unoccupied states above the Fermi level (Figure 1a). XAS technique has two very important aspects which are the site and the symmetry selectivity. The site symmetry is due to the specific binding energy of the core electron and the localized character of the excitation. The technique is also a local probe since the excitation is localized and the dipole selection rule is applicable and gives the symmetry dependence of each feature of the spectra.

This X-ray absorption cross section μ(E) is most generally given by the Fermi's golden rule

$$\mu(E) \propto \sum_f \left|\langle f|H|i\rangle\right|^2 \delta\left(E_i - E_f + h\nu\right) \tag{2}$$

where, and denote the initial and final states and their energies. In XAS matrix elements, the final state is localized.

- H is the whole system Hamiltonian, in the dipole approximation,
- The dipole selection rules can be considered.

Thus, equation (2) becomes:

$$\mu(E) \propto \sum_f \left|\langle f|\vec{\varepsilon}.\vec{r}|i\rangle\right|^2 \delta\left(E_i - E_f + h\nu\right) \tag{3}$$

Only the dipole contribution to the total cross-section has been considered in Equation (3). By exciting an atom using an X-ray source, the electrons configuration of the atom is changed; one electron, usually a core-shell electron, or more electrons populate unoccupied bound or continuum states (figure 1). The success of this spectroscopy lies in the fact that the photoelectron acts as very sensitive probe that can "feel" the charge distribution and the arrangement of the neighbouring atoms around the absorbing atom, or, in the other words, it can feel the chemical environment of the neighbouring atoms. When the photon energy is not high enough, the photoeffect in one of the core shells can occur. It results in the step like shape of the absorption spectrum: the increased photoabsorption cross-section due to the knocking-out of an electron is called absorption edge.

One way of understanding this excitation process in a bound atom is describing it by means of multiple scattering (MS): the photoelectron's wave is scattered on atoms surrounding the absorbing atom. The cross-section of a bound atom therefore depends on the positions and types of the neighbours and is different from that of an isolated atom. The photoelectrons can populate either unoccupied bound states or low-lying continuum states. The part of the spectrum (Figure 2) concerned is the XANES.

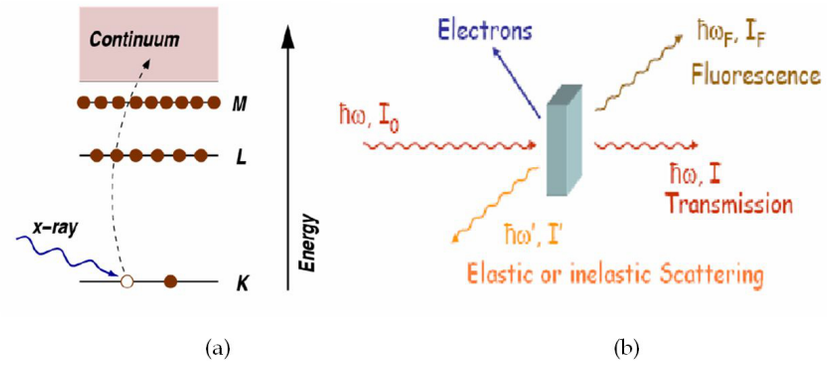

Figure 1. a) The absorption of X-ray by an atom promoting a core-level electron (K) into the continuum, (b) X-ray radiation and matter interactions [10].

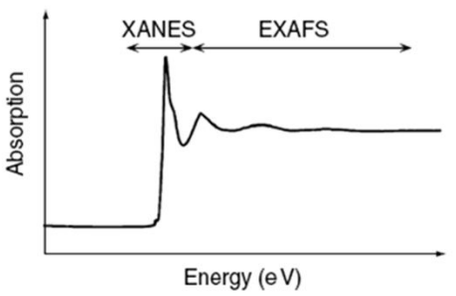

Figure 2. Schematic illustration of an X-ray absorption spectrum, showing the structured absorption that is seen both within 50 eV of the edge (the XANES) and for several hundred to >1,000 eV above the edge (the EXAFS) [11].

On its high energy end, XANES extends up to Extended X-ray Absorption Fine Structure (EXAFS) [12]. The limiting energy that divides XANES from EXAFS is by no means exactly defined since the transition from the one regime to the other is smooth. As a rule, near-edge structure ends approximately where the electron wavelength equals the distance from the absorbing atom to its nearest neighbours [12, 13], which usually means about 40–50 eV above the edge. In the XANES regime, the electron's kinetic energy is small and the scattering on the neighbouring atoms tends to be strong, while the effect of the scatterers becomes smaller at higher energies; in EXAFS region, the photoelectrons are only weakly scattered. Albeit EXAFS represents the most understood part of XAS, XANES is the only part used in this study to characterize carbon nanostructures and its theoretical study is the aim of the next paragraph.

When attention is paid to scattering form of potentials of several objects (systems of particles), each of them makes a non-zero contribution only within a spherically non-overlapping scattering region of finite radius (Figure 3a). The total potential V is given by:

$$V = \sum_i \upsilon^i \tag{4}$$

Outside the spherical regions – in the interstitial region – the potential is set to zero. This approximation presented in Figure 3b is known as the muffin-tin approximation. The scattering parameters of each of the scatterers, namely the scattering amplitudes and phase shifts, are determined separately for each scatterer and are therefore pure atomic quantities. The propagation of a photoelectron in such muffin-tin potential V is described by the Hamiltonian:

$$H = H_0 + V \tag{5}$$

is the kinetic-energy operator. The stationary solution with the energy E is given by:

$$(E - H_0)\left|\psi\right\rangle = V\left|\psi\right\rangle \tag{6}$$

Solving the "inhomogeneous" Equation (6) by means of the Green's functions and to be more specific, if $\langle r \mid \varphi \rangle$ is the solution of the "homogeneous" part of Equation (6)

$$(E - H_0)\left\langle r\middle|\varphi\right\rangle = 0 \tag{7}$$

The free-electron Green's function G_0 is defined by relation

$$(E - H_0)G_0(r, r'; E) \equiv (\Delta + k^2)G_0(r, r'; E) = \delta(r - r') \tag{8}$$

then the general solution of Equation (6) is given as a sum of the solution of the *homogeneous* equation and the particular solution [14, 15] is given below:

$$\left\langle r\middle|\psi\right\rangle = \left\langle r\middle|\varphi\right\rangle + \int d^3r' G_0(r, r'; E)\left\langle r'\middle|V\psi\right\rangle \tag{9}$$

For the photoelectron only weakly scattered by the potential V (XANES), the solution $\langle r \mid \psi \rangle$ is close to the free-electron solution $\langle r \mid \varphi \rangle$. Furthermore, when V is identically zero everywhere, the exact equality $\langle r \mid \psi \rangle = \langle r \mid \varphi \rangle$ holds, as expected. It is clear from Equations (7) and (9) that there are solutions of the total Hamiltonian, that $\mid \psi \rangle$ have the same energy as $\mid \varphi \rangle$ only when elastic scattering is considering.

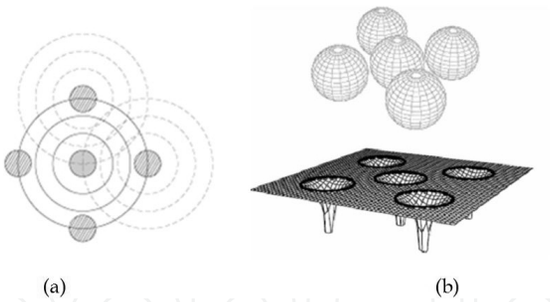

Figure 3. a) The wave function of the photoelectron is scattered on the neighbouring atoms (b) the muffin-tin potential consisting of non-overlapping spherical regions [14].

The formal solution of the operator on equation (8) is given by the Lippman-Schwinger equation [15, 16],

$$|\psi\rangle = |\varphi\rangle + \frac{1}{E - H_0 \pm i\eta} V |\psi\rangle \tag{10}$$

The operator $\frac{1}{E - H_0 \pm i\eta}$ can be considered as $\frac{1}{E - H_0}$ modified by an imaginary term in the denominator $i\eta$with ηinfinitesimally small and positive. The comparison of equations (9) and (10) reveals the following equality (11)

$$G_0^{\pm}(r, r'; E) = \langle r | \frac{1}{E - H_0 \pm i\eta} | r' \rangle \tag{11}$$

The operator $\frac{1}{E - H_0 \pm i\eta}$ can be considered as $\frac{1}{E - H_0}$ modified by an imaginary term in the denominator $i\eta$with ηinfinitesimally small and positive. The comparison of equations (11) and (12) reveals the following equality (11)

and then

$$G_0^{\pm} = \frac{1}{E - H_0 \pm i\eta} \tag{12}$$

And obviously,

$$\langle r | G_0^{\pm} | r' \rangle = G_0^{\pm}(r, r'; E) = \frac{-1}{4\pi} \frac{\exp(\pm ik(r - r')}{|r - r'|} \tag{13}$$

where $k = \sqrt{E}$, G_0^+ and G_0^- describe how outgoing and incoming spherical waves propagate in free space, respectively. The Lippman-Schwinger equation can be solved formally if the transition operator T is introduced [15, 16],

$$V|\psi\rangle = T|\varphi\rangle \tag{14}$$

The propagator of the whole system can be defined as:

$$G(E) = \frac{1}{E - H_0 - V + i\eta} \tag{15}$$

One can deduce that:

$$G = G_0 + G_0 T G_0 = G_0 + G_0 V G_0 \tag{16}$$

and

$$T = V + V G_0 V = V + V G V \tag{17}$$

The total potential is $V = \sum_i v^i$ and the potentials v^i are non-overlapping, the transition operator of individual atoms is:

$$t^i = v^i + v^i G_0 v^i \tag{18}$$

The propagator matrix G written in equation (16) can be extended by:

$$G = G_0 + G_0 T G_0 + G_0 T G_0 T G_0 + \ldots \tag{19}$$

where

$$T = \sum_i t^i \tag{20}$$

This last equation is a geometric series and therefore:

$$G = (1 - G_0 T)^{-1} G_0 \tag{21}$$

In the multiple scattering theory, the hard work is in computing the Green's function G. The function G describes all the possible ways for a photoelectron to interact with the surrounding atoms, G_0 is the function that describes how an electron propagates between two points in space. T is the parameter that denotes how a photoelectron scatters from a neighbouring atom.

The multiple scattering formalism used with the paradigm shift theorem, leads to another formulation of the Fermi's Golden law given by Equation (21):

$$\mu(E) \propto -\frac{1}{\pi} \operatorname{Im} \left\langle i \left| \vec{\varepsilon} \bullet \vec{r}' G(r', r; E) \vec{\varepsilon} \bullet \vec{r} \right| i \right\rangle \tag{22}$$

This last expression of the Fermi's Golden rule is very efficient, because there is no more sum over final states. This law is, in some cases, expressed with the wave functions that can be determined from electronic-structure calculations. In band structure calculations in crystals for example, the eigenstates and eigenvalues of the total Hamiltonian *H* can be obtained using either Bloch and Wannier functions or Linear Combinations of Atomic Orbitals (LCAO) methods [17]. In that case, the state vectors $|i\rangle$ and $|f\rangle$ represent the stationary solutions of electrons moving in a periodic potential.

Conversely, the situation can be faced using the MS theory. According to the paradigm shift theorem, there is a relation between the Green's function *G (r', r, E)* and the final state vector:

$$n(E) = -\frac{1}{\pi} \operatorname{Im} G(r', r, E) = \sum\nolimits_f \left| f \right\rangle \delta(E - E_f) \left\langle f \right| \tag{23}$$

As with the total Green's function *G(E)* which consists of the free propagator $G_0(E)$ and the term describing the propagation of the scattered wave, the total density of states can also be divided into two parts as shown in equation (23). The "atomic" part, $n_0(E)$ and the change due to the scattering, $n_{scat}(E)$:

$$n(E) = n_0(E) + n_{scat}(E) \tag{24}$$

It is clear that the density of final states is changed because of the presence of the scatterers. Thus, the behaviour of the physical system can be reinterpreted. The solutions can be understood either as stationary solutions of the total Hamiltonian or as solutions that are changed by the multiple scattering from surrounding atoms.

3. Electron microscopy observations

3.1. SEM Observations

The SEM morphology images are performed on an XL30S-FEG PHILIPS working at 3 kV. SEM images clearly illustrated in different figures, show that the CNTs synthesized in this study display widely different morphologies according to the values and the concentrations of variable parameters. Within medium plasma power (around 150 W); carbon nanotubes are grown with graphitic planes in a parallel direction to the fiber axis. These samples however display different mutual orientations.

Highly oriented films are obtained under optimized conditions as represented in figure 4a, consisting in the evaporation of TM which is Co or mixture of Co and Fe. The pressure of the chamber is 15 mbars. CNTs obtained are very appropriate for applications like electric field emission devices, as they require samples aligned perpendicularly on a flat substrate. But those obtained in figure 4b, are poorly oriented. These figures clearly show a general view of poorly oriented CNTs, with important physical defects. They can have another area of applications. Carbon nanostructures defects are useful in many fields of applications.

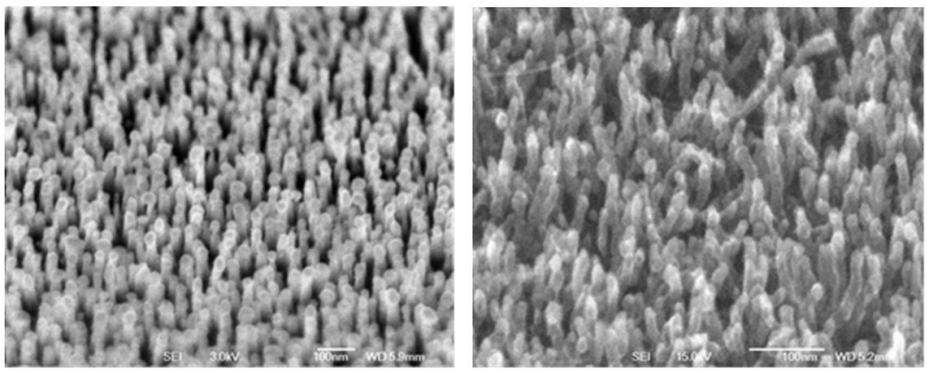

(a) (b)

Figure 4. SEM images: (a) highly oriented carbon nanotubes obtained under optimized conditions (b) poorly oriented carbon nanotubes

Figure 4(b) shows poorly oriented nanotubes films obtained with more defects. Anyway the presence of hot filaments heated around 2200 K must be stressed. They provide hydrogen radicals that are very reactive towards all kinds of amorphous carbon. Thus, carbon surrounds not only the particle but is also spread onto the surface of the sample. Figures 5 and 6 show the impact of the concentration of ammonia in synthesis chamber. In the particular case of CNTs, Table 1 shows important differences with respect to the ammonia concentration. First of all, the density decreases when the ammonia concentration increases. Secondly, the length distribution changes. The different values are: 300 to 450 nm for 0% of ammonia concentration, for 1% it is 250 to 500 nm and 800 to 3000 nm for 3%. The morphological defects are also related to ammonia concentration. They are important at 0 and 3%.

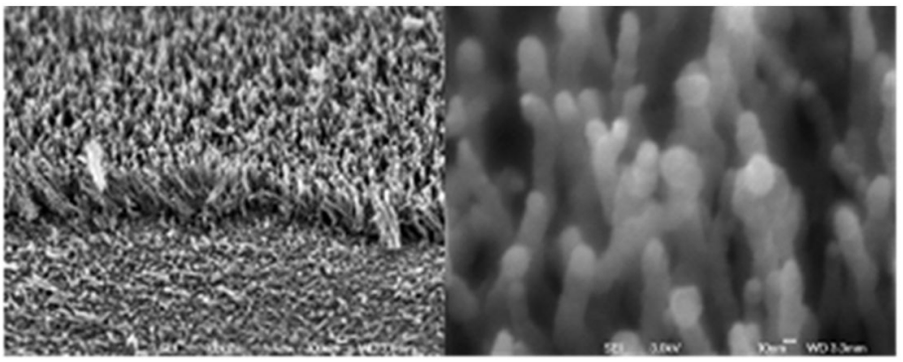

Figure 5. SEM images with low and high magnification at 0% NH_3.

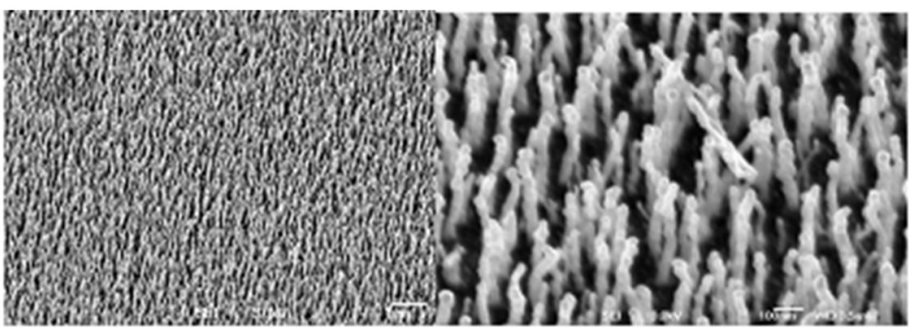

Figure 6. SEM images with low and high magnification at 1% NH_3.

Sample	% NH_3	Density (μm^{-2})	Mean diameter (nm)	Length distribution
1	0	290	20 ± 5	300 - 450
2	1	50	20 ± 5	250 - 500
3	3	3	20 ± 5	800 - 3000

Table 1. Main experimental morphological and correlation data determined from SEM and TEM observation for CNTs.

In spite of the fact that SEM analysis gives valuable information in morphological and structural characterization of CNTs, it is however not sufficient to establish the ultimate nature of carbon nanotubes. It is easy to confuse only on the basis of SEM observations carbon nanotubes from nanofibers. Thus, one proceeds to TEM analysis of the samples to have deeper information on obtained CNTs.

3.2. TEM observations

The samples are examined by TEM in order to complete the SEM study by controlling the density and the morphology of CNTs deposited. TEM observations are performed on a TOPCON 002B microscope operating at 200 keV. Each sample is scratched with a diamond tip and the material is directly pulled onto the membrane for observations. The carbon membrane is drilled with holes in order to get more accurate observations. TEM micrographs clearly illustrate that nanotubes obtained display widely different morphologies according to some variable parameters. And it is possible to control the morphology. Within the medium value of the plasma power, as shown with SEM study, carbon nanotubes are yet grown. These samples however display different mutual orientations. The highly oriented films are obtained under optimized conditions and poorly and medium oriented films are also obtained, showing more defects.

One of the very important observations is that each carbon nanotube grown has TM nanoparticles at its top or its base [18, 19]. The TEM observations show at the same time that the surface of the nanotubes exhibits an amorphous structure due to wall surface defects (Figure 5a and Figure 5b). The outer diameters of the CNTs are directly determined from TEM images with high accuracy. Thus the mean outer diameter is 20 nanometers the smallest being 10 nm corresponding surely to SWCNTs or to a few number of walls. The upper values, may account for outer diameters of MWCNTs.

The analysis of TEM images lead to extensive values of length, varying from 100 to 400 nanomaters, as illustrated in Table 1. The density of nanotubes spreads also in a very large range. It ranges between 350 to 1000 μm. Figure 7 shows CNTs completely detached from the substrate with catalyst paticles on one end (figure 8), and the graphitic end of attachment to the substrate.

Unfortunately, TEM images of CNTs do not give the opportunity to determine the exact number of walls of each sample of CNTs (Figure 7a). This deficiency is the result maybe of defects. In this way, mutually aligned tubes of different densities are obtained, depending on the ammonia concentration in the reactive gas mixture. TEM images of CNTs show that the mean diameter is 25 nm and few micrometers in length. From the TEM image one could see that CNTs are very thin like a broadcast needles on the floor. The absence of TEM analysis can lead to wrong conclusion in the case of carbon nanomaterials. It is the most important and most reliable technique for correctly identifying the nature and the form of carbon nanomaterials. However, it remains some missing information. TEM images of CNTs and CNFs clearly distinct, but it is quite difficult to know the exact number of walls.

HRTEM is now capable of imaging individual atoms in nanostructures with subangström resolution as shown by Cowley and Liu [20]. The continue development of new tools is critical to the pace of further progress in nanoscience and technology, they provide the “eyes” to see and the “fingers” to handle nanostructures. In the nearer term, the greater need is to provide laboratory researchers with the instruments and tools to discover and investigate new chemical, physical, and biological phenomena and applications.

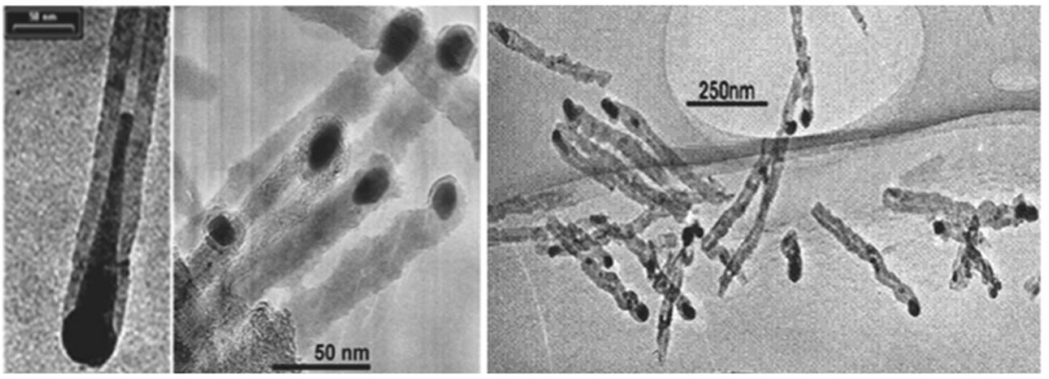

Figure 7. CNTs TEM images with TM particles inserted at one end: (a) CNT highly oriented, (b) CNTs medium oriented and (c) CNTs sample synthesized with 1% of NH3. The two ends of each CNT are well observed detached from the substrate. One end has graphitic structure (half fullerene) and the other has a TM particle inserted in the tube.

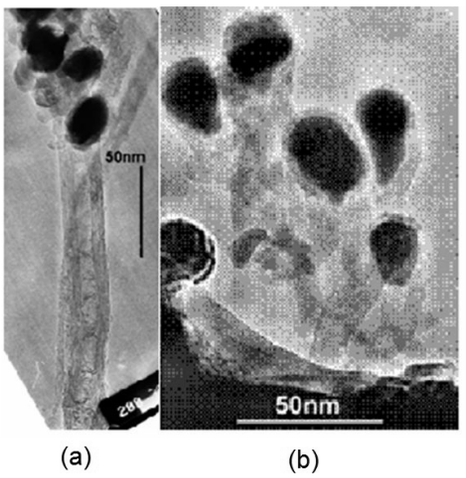

Figure 8. CNTs with metal particles on top: a) highly oriented and b) poorly oriented.

In the longer term, those tools will evolve into inexpensive, easy-to-use sensors and/or diagnostic devices with numerous applications.

3.3. SEM and TEM Characterization and discussions

A perfect CNT is an abstraction, because the hexagonal structure sp^2 forms layers with different types of alterations as shown in literature. These alterations can come from the growth mode, from the deposit on a substrate, or they can be the result of a heat or chemical treatment. An important consequence of these defects on surface morphology that needs to be pointed out is the roughness of CNTs surface. The defects are in general very important

because they can modify the electronic properties of the nanostructure, and so, can be seen as a feature that can influence nanostructures applications [21]. Generally, a defective site has a high chemical reactivity, in other words, this site is chemical reactions favoured [18]. Thus CNTs and CNFs with poor orientation, and which have many defects are not appropriate for applications in field emission devices, but can have other important applications like functionalization. In most cases, TEM investigations and seldom in SEM's, it is shown that the catalyst metal particles are attached to the nanostructures top end (nanofibers or nanotubes), or found inside the nanostructures (nanofibers, nanotubes and nanoparticles) or at last in the sidewalls for all varieties obtained (figures 7 and 8).

According to aiming applications, the presence of ultrafine cobalt or cobalt/iron nanoparticles of various diameters at the top of nanostructures can have negative effect. In particular in the case of emission of electrons or electric field, the particles need to be carried off. Thus, the purification of nanostructures needs to be one of crucial parts of synthesis process.

Single walled carbon nanotubes come often as tightly bundles of single walled nanotubes entangled as curly locks is often seen in literature. The packing of the nanotubes inside a bundle is not observed in specific case helping therefore to differentiate SWCNTs from MWCNTs. CNTs are simply observed in SEM images as tubes forest with poorly, medium or highly orientation depending on synthesis conditions, in particular the concentration of ammonia. It is possible that CNTs grown by HF PE CCVD be only MWCNTs. The second hypothesis is that defects or the presence of TM particles or other contaminants in nanostructures sidewalls, preclude SWCNTs present to gather in bundles. The third assumption can be that SWCNTs are present in samples, but these CNTs with lowest outer diameter which is 10 nm cannot form bundle because of orientation problems. The CNTs with the lowest outer diameter are depicted on two samples namely Nanot 29 and FLN 2. Nanot 29 is poorly oriented while FLN 2 has the high orientation as seen in figure 7. But in both cases, nanotubes are not gathering in bundles. Partially, the conclusion is that the degree of orientation is not precluding nanotubes to form bundles. But the absence of bundles in the case of eventual SWCNTs may be induced by defects or the attachment of catalytic nanoparticles. This situation may be solved by additional chemical or heat treatment stage for purification of obtained samples before any electron microscope imaging.

TEM gives direct insight into the structure of carbon nanomaterials and can help to identify the material or the phase correctly. Without observations by TEM, one may lead to wrong or incorrect conclusions. It is the most important and most reliable technique for correctly identifying the nature and the form of carbon nanomaterials, in spite of the fact that the information that can be extracted is not straight-forward, since the preparation of TEM samples may mask observation of the nanostructures of lower size, or the possibility of the projection of artefacts. TEM has become useful for *in situ* microscopy, for observing dynamic processes at the nanoscale nanomeasurements which directly correlate physical properties with structures, holographic imaging of electric and magnetic fields, quantitative chemical mapping at subnanometer resolution and for ultra-high resolution imaging. The main characteristics of CNTs obtained are given in Table 2.

Understand of the growth mode of CNSs in general is among the imperatives in their characterization and can lead to the growth modelling. In the case of CNTs or CNFs, two dominant growth modes have been observed in SEM and TEM images. The tip growth mode and the base growth mode, which are in agreement with literature. In tip growth mode, the transition metal nanoparticle catalyzing the growth of the carbon nanostructure remains at the top of the nanostructures. The adhesive forces between the substrate and the catalyst nanoparticles seem typically too small and the particles are lifted up as the CNTs or CNFs grow. The process takes place till the temperature is upper, before the cooling.

Sample	Carbon nanostructure	Outer diameter (nm)	Inner diameter (nm)	Lenth (nm)	Density (μm)
I Nanot29	CNTs (poorly oriented)	10	/	/	/
II Nanot31	CNTs	30	9	375	400
III Nanot42	CNTs (highly oriented)	25	5	400	349
IV FLN1	CNTs (medium oriented)	/	/	100	/
V FLN2	CNTs (highly oriented)	10	4	187	1000

Table 2. Main characteristic parameters of the carbon nanotubes synthesized.

4. XANES Characterization of CNTs

4.1. Assignments of peaks of CNTs

Owing to the alignment of nanotubes with a specific orientation of the σ bonds, it is expected that the absorption on the C K-edge, using total electron yield (TEY) and partial electron yield (PEY), knowing that the last is less surface-sensitive, will present angular selectivity when considering the specific $\pi \rightarrow \pi^*$ transition. The potential for the use of XANES as an unambiguous method of determining carbon nanostructures quality, orientation and contamination is due to the fact that one measures directly the unfilled electronic states and thus the chemical bonding state of the target atoms.

The assignment of features of XANES spectra of our samples of CNTs leads to the following tables (table 3 and table 4).

Annealed and potassium-contaminated CNTs at grazing incidence Nanot29_OE29				
Peak name	**Peaks**	**Binding energy (eV)**	**Kinetic energy (eV)**	**Final-state band and Brillouin-zone**
A	285.50	285.08	1199.32	π_0 near Q
	286.53	287.14	1197.26	free-electron-like interlayer states + adsorption
A''	288.40	288.52	1195.88	free-electron-like interlayer states + adsorption
A'''	288.70	289.68	1194.72	free-electron-like interlayer states + adsorption
A''''	290.70	290.60	1193.80	free-electron-like interlayer states + adsorption
C-H Exc.	291.76	291.44	1192.96	Exciton
B	292.65	292.20	1192.20	σ_1, σ_2: Γ→Q
C	295.50	294.55	1189.85	π_0 or π_1 near Γ
D	297.80	298.05	1186.35	
P''	297.51	296.35	1188.05	Potassium L_2 level
E	303.50	301.75	1182.65	σ_7 near Q
F	307.50	306.50	1177.90	σ_9 near Q
G	308.50	309.72	1174.68	
H	316.50	314.10	1170.30	π_4 near Q
I	329.00	329.00		
J	333.00	333.00		
P	296.60	296.95	1187.45	Potassium L_2, L_3 level
P'	299.83	299.37	1185.03	Potassium L_2-L_1 levels
R = (A+C+H+P'')/(B+D+E+F+G) = 0.863 $R=(\pi/\sigma)_{tot}$				

Table 3. Main features' parameters for annealed and potassium-contaminated CNTs XANES spectrum at grazing incidence.

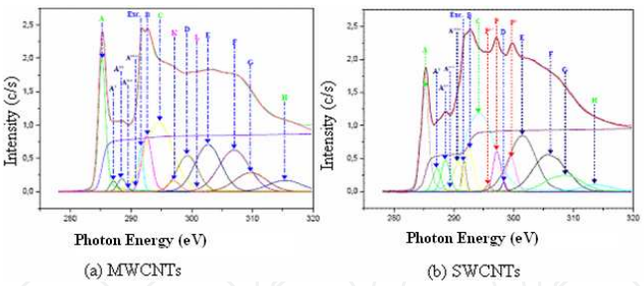

Figure 9. CNTs experimental and calculated superimposed XANES spectra at grazing incidence from unannealed samples: (a) without potassium contamination, (b) with potassium contamination.

Annealed and potassium-contaminated CNTs at normal incidence Nanot29_OE36				
Peak Name	**Peaks**	**Binding energy (eV)**	**Kinetic energy (eV)**	**Final-state band and Brillouin-zone**
A	285.50	285.20	1199.20	π_0 near Q
A'	286.53	287.31	1197.09	free-electron-like interlayer states + adsorption
A''	288.40	288.67	1195.73	free-electron-like interlayer states + adsorption
A'''	288.70	289.68	1194.72	free-electron-like interlayer states + adsorption
A''''	290.70	290.35	1194.05	free-electron-like interlayer states + adsorption
C-H Exc.	291.76	291.64	1192.76	Exciton
B	292.65	292.40	1192.00	σ_1, σ_2: Γ→Q
C	295.50	294.67	1189.73	π_0 or π_1 near Γ
D	297.80	298.30	1186.10	
P''	297.51	296.20	1188.20	Potassium L_2 level
E	303.50	301.85	1182.55	σ_7 near Q
F	307.50	306.54	1177.86	σ_9 near Q
G	308.50	310.00	1174.40	
H	316.50	314.30	1170.10	π_4 near Q
I	329.00	329.00		
J	333.00	333.00		
P	296.60	297.20	1187.20	Potassium L_2, L_3 level
P'	299.62	299.37	1184.78	Potassium L_2-L_1 levels
R = (A+C+H+P'')/(B+D+E+F+G) = 0.962				

Table 4. Main features' parameters for annealed and potassium-contaminated CNTs XANES spectrum at normal incidence.

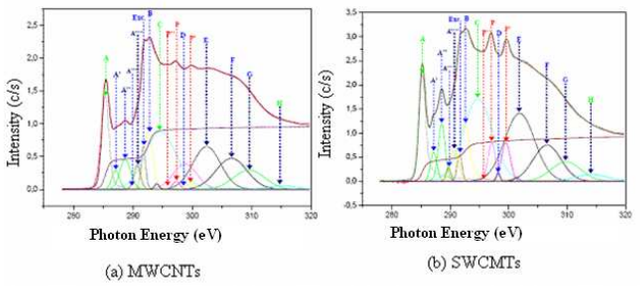

Figure 10. Contaminated CNTs experimental and calculated superimposed XANES spectra at normal incidence from annealed (550°C) samples: (a) sample is sensitive to thermal annealing; (b) sample is less sensitive to thermal treatment.

It is elementally selective by the tunability of the synchrotron X-ray source and sensitive to the bond order according to optical dipole selection rules. In the light of the XANES and HOPG spectra used as a starting point model, a prior annealing of the samples prevents the increase of intensity in the free-electron-like interlayer states region of the spectra, clarifying that these features are not intrinsic.

4.2. Orientation tendency parameter of CNTs R(α)

The parameter R(α) deduced from the fitting of the carbon K-edge absorption spectra by the ratio of the intensity of π*-type features (A+C+K+H) over σ*-type features (B+D+E+F+G+L), is defined to determine more quantitatively the respective contributions of the σ* and π* transitions at incidence angle α, and it is given by the relation below:

$$R(\alpha) = \frac{A + C + H + K}{B + D + E + F + G + L} \tag{25}$$

or

$$R(\alpha) = \frac{\sum \pi}{\sum \sigma} \tag{26}$$

This ratio or parameter calculated in Table 3 and Table 4, is indicative of the orientation tendency of the CNTs orbitals, and by the way, the graphite layer. In the related case, R(α) equals 0.868 in grazing incidence and 0.962 in normal incidence. It is expected to be maximum and minimum whens the XANES spectrum is recorded at normal and grazing incidence, respectively. In good agreement, R(α) in grazing incidence and R(α) in normal incidence are quoted to 0.868 and 0.962, respectively.

A prior annealing of the samples has prevented the increase of intensity in the free-electron-like interlayer states band region of the spectra, clarifying that these features are not intrinsic as shown elsewhere [8, 9]. But there is not total extinction observation of the σ* band at 285.5

eV at normal incidence, the residual intensity of that peak at α=0 is probably due to either the uncompleted polarization of the synchrotron X-ray light beam or sample misalignment. The R(α) parameter in Table 9 equals 0.078. Thus, unambiguously the π orbitals lie perpendicular to the graphene sheet.

As a general trend, the *R(α)* parameter values at normal incidence are greater than those at grazing incidence for CNTs contrary to those of the HOPG [24, 25]. The obtained CNTs are classified in three groups according to its values according to table 5:

- Those with poor orientation,
- The other with medium range orientation,
- The last group which is formed of high CNTs.

For poorly oriented CNTs, the discrepancy between the two values (NI and GI) is too small.

It increases towards high oriented CNTs according to Table 5 bellow.

CNTs	CNTs1	CNTs2	CNTs3
GI	0.778	0.962	0.975
NI	0.732	0.882	0.665
ΔR	0.046	0.079	0.310
Observation	Poor Oriented	Medium Oriented	High Oriented

Table 5. The values of *R(α)* of three samples of CNTs. The discrepancy of these values at normal incidence (NI) and grazing incidence (GI) allows the classification of CNTs in: poor, medium and high oriented.

5. CNSs contamination

If the defects like: topological defects (the occurrence of pentagons and heptagons), the sp^3 hybridized carbons atoms and incomplete bonding that have slight changes that can be neglected, are not taken into account, it is observed that some features present in Figure 9 (a) are not found in Figure 9 (b), especially peaks K and L, and are replaced by P, P′ and P″. These new peaks are not intrinsic to CNTs. They are the result of contamination which can be considered as accidental adsorption of atoms, molecules or radical compounds, in agreement with SEM and TEM analysis, where it is not found bundles of CNTs as it may be, according to literature. Among the reasons of the presence of non-intrinsic features in XANES spectra is the presence of TM particles as proved by SEM and TEM. Actually, it is known that the features attributed to the so-called free-electron-like interlayer states in the graphite and other carbon nanostructures are also due to contamination [8, 9]. The peaks P, P′ and P″ are assigned to adsorbed potassium atoms according to features parameters [9, 23].

6. Conclusion

We investigate qualitatively and quantitatively the properties of carbon nanotubes synthesized by HF PE CCVD on SiO_2/Si(100) substrate using electron microscopies and X-ray absorption spectroscopy near-edge. According to SEM and TEM images and XANES spectra, CNTs are highly oriented under optimized conditions, notably when the ammonia concentration is 1% of gases mixture, but when this concentration is different (0 or 3%), samples are full of defects. Highly oriented CNTs are obtained under optimized conditions consisting of the evaporation of Co or mixture of Co and Fe or other TM element. The pressure of the chamber is 15 mbars. The CNTs obtained are very appropriate for applications like electric field emission devices when ammonia concentration is 1% of gases mixture, because such devices need CNSs samples oriented perpendicular to the plan of the substrate. The analysis of TEM images reveals that the length of each CNT varies from 100 to 400 nm, and their density is included between 350 and 1000 μm. The mean outer diameter depends on the size of catalyst particle. Its value is around 20 nm while the smallest value is 10 nm corresponding surely to SWCNTs.

Perfect CNTs are an abstraction or a creation of the mind, because of the hexagonal structure of sp^2 carbon atoms, which form the graphite layers, with always alterations. These defects are important because they often modify the electronic properties of the nanostructures, and can influence their applications. SWCNTs come often as tightly bundles entangled as curly locks is seen in literature, but these packing of the nanotubes inside bundles is not observed in specific case helping to differentiate SWCNTs from MWCNTs. CNTs are simply observed in SEM images as tubes with poorly, medium or highly oriented, depending on synthesis conditions. The degree of orientation is not precluding nanotubes to form bundles. But the absence of bundles in the case of eventual SWCNTs may be induced by defects or the attachment of catalytic nanoparticles. In particular, in the case of emission of electrons or electric field, these nanoparticles need to be removed. Thus, the purification of nanostructures needs to be one of crucial parts of synthesis process. This situation may be solved by additional chemical or heat treatment of obtained sample before electron microscope imaging and spectroscopic.

The contamination is due to atoms, radicals or molecules adsorbed of many species present or formed during synthesis phase, among them are oxygen (O); water and TM (catalyst). But the spectral features P, P′ and P′′ observed in many spectra, are assigned to 7potassium (K) contamination. This potassium present in samples might come from the beam lines contamination. These results elucidate that the CVD is one of the best techniques for synthesis of the CNSs for multiple purposes.

As a summary, the morphology and the structure of CNTs obtained by HF PE CCVD on SiO_2/Si(100) depend widely on the transition metal used as catalyst, and the experimental parameters during the growth process. It appears that synthesized CNTs can be used for many purposes according to growth conditions which determine their properties. Those with electronic defects are appropriated for functionalization because of their high chemical reactivity. Those with small outer diameter are also characterized by high chemical reactivity and can also be used in functionalization. On the other hand, CNTs with highly oriented configuration are very ideal in field or electrons emission devices manufacture.

Acknowledgements

The author would like grateful acknowledge Pr Motapon Ousmanou, Pr Mane Mane J., Dr Ben-Boli G. H. and Dr Tiodjio Sendja B. for many helpful discussions.

Author details

Rolant Eba Medjo*

Address all correspondence to: emeroch@yahoo.fr

Department of Physics, Faculty of Science, University of Douala, Republic of Cameroon

References

[1] Dresselhaus, M. S., Dresselhaus, G., & Eklund, P. C. (1996). *Science of Fullerene and Carbon Nanotubes*, Academic Press.

[2] Ebbesen, T. W. (1997). *Carbon Nanotubes: Preparation and Properties*, Chemical Rupper Corp, Boca Raton, FL.

[3] Zuttel, A., & Sudana, P. (2002). *International Journal of Hydrogen Energy*, 27, 203.

[4] Taschner, C., Pacal, F., Leonhardt, A., Spatenka, P., Bartsch, K., Graff, A., & Kaltofen, R. (2003). *Surface and Coatings Technology*, 81, 174.

[5] Thiodjio Sendja, B., Eba Medjo, R., Mane Mane, J., Ben Bolie, G., Diop, D., & Owono Ateba, P. (2010). A GISAXS Study of Angular dependence of Carbon Nanotubes grown on a plain substrate by dc HF CCVD process. *Phys. Scr.*, 82, 025601.

[6] Rosenberg, R. A., Love, P. J., & Rehn, V. (1986). Polarization-dependent C(K) near-edge x-ray-absorption fine structure of graphite. *Phys. Rev. B*, 33, 4034.

[7] Shimoyama, Iwao, Wu, Guohua, Tetsuhiro, Sekiguchi, & Yuji, Baba. (2001). Study of electronic of graphite-like carbon nitride. *Journal of Electron Spectroscopy and Related Phenomena*, 114-116, 841-848.

[8] Zhong, J., Liu, C., Wu, Z. Y., Mamatimin, Kurash I., Cheng, H. M., Gao, B., & Liu, L. (2005). XANES Study of Carbon Based Nanotubes. *High Energy Physics and Nuclear Physics*, 29, 97.

[9] Eba Medjo, R., Thiodjio Sendja, B., Mane Mane, J., & Owono Ateba, P. (2009). A study of carbon nanotube contamination by XANES spectroscopy. *Phys. Scr.*, 80, 045601.

[10] NIST. *Physical Reference Data*, http://physics.nist.gov/PhysRefData/XrayMassCoef/cover.html.

[11] Joly, Y. http://www.ned.cnrs.fr.

[12] Koningsberger, D. C., & Prins, R. (1988). X-Ray Absorption- Principles, Applications, Techniques of EXAFS, SEXAFS and XANES. *Chemical Analysis*, 92, Wiley.

[13] Koningsberger, D. C., & Prins, R. (1992). X-Ray Absorption- Principles, Applications, Techniques of EXAFS, SEXAFS and XANES. *Wiley-Interscience*, New-York.

[14] Mihelic, A. (2002). http://www.p-ng.si/~arcon/xas/xanes/xanes-theory.pdf.

[15] Sakurai, J. J. (1994). *Modern Quantum Mechanics*, Rev. Ed., Addison-Wesley.

[16] Merzbacher, E. (1970). *Quantum Mechanics*, John Willey.

[17] Ashcroft, N. W., & Mermin, N. D. (1976). *Solid state physics*, Saunders College.

[18] Eba Medjo, R., Thiodjio Sendja, B., Mane Mane, J., & Owono Ateba, P. (2009). XAS study of orientated carbon nanotube films. *Phys. Scr.*, 80, 055602.

[19] Mane Mane, J. (2007). *Habilitation à Diriger des Recherches*, Université Louis Pasteur de Strasbourg.

[20] Cowley, J. M., & Liu, J. (1993). Contrast and resolution in REM, SEM and SAM. *Surface Science*, 298, 456.

[21] Bonard, J-M. (2005). Carbon nanostructures by Hot Filament Chemical Vapor deposition: Growth, properties, applications. *Thin Solid Films*, 501, 8-14.

[22] Stöhr, J. (1992). *NEXAFS Spectroscopy*, Springer, Berlin.

[23] Sasaki, S. (1984). KEK, National Laboratory for High Energy Physics. *Report*, 83, 22.

[24] Eba Medjo, R. (2011). *Structural and morphological characterization of carbon nanostructures synthesized by chemical vapour deposition using spectroscopic techniques and electron microscopies*, Thesis, University of Yaounde I.

[25] Eba Medjo, R. (2011). Carbon Nanotubes Synthesis. *In: Marulanda, J. M. (ed) Carbon Nanotubes Applications on Electron Devices*, Rijeka: Intech, 3-36, Available from, http://www.intechopen.com/books/carbon-nanotubes-applications-on-electron-devices/carbon-nanotubes-synthesis, accessed 01 august 2011.

IntechOpen